

DESY-09-059
21st April, 2009

Scaled momentum distributions of charged particles in dijet photoproduction at HERA

ZEUS Collaboration

Abstract

The scaled momentum distributions of charged particles in jets have been measured for dijet photoproduction with the ZEUS detector at HERA using an integrated luminosity of 359 pb^{-1} . The distributions are compared to predictions based on perturbative QCD carried out in the framework of the modified leading-logarithmic approximation (MLLA) and assuming local parton-hadron duality (LPHD). The universal MLLA scale, Λ_{eff} , and the LPHD parameter, κ^{ch} , are extracted.

The ZEUS Collaboration

S. Chekanov, M. Derrick, S. Magill, B. Musgrave, D. Nicholass¹, J. Repond, R. Yoshida
*Argonne National Laboratory, Argonne, Illinois 60439-4815, USA*ⁿ

M.C.K. Mattingly
Andrews University, Berrien Springs, Michigan 49104-0380, USA

P. Antonioli, G. Bari, L. Bellagamba, D. Boscherini, A. Bruni, G. Bruni, F. Cindolo,
M. Corradi, G. Iacobucci, A. Margotti, R. Nania, A. Polini
INFN Bologna, Bologna, Italy^e

S. Antonelli, M. Basile, M. Bindi, L. Cifarelli, A. Contin, S. De Pasquale², G. Sartorelli,
A. Zichichi
University and INFN Bologna, Bologna, Italy^e

D. Bartsch, I. Brock, H. Hartmann, E. Hilger, H.-P. Jakob, M. Jünger, A.E. Nuncio-Quiroz,
E. Paul, U. Samson, V. Schönberg, R. Shehzadi, M. Wlasenko
Physikalisches Institut der Universität Bonn, Bonn, Germany^b

N.H. Brook, G.P. Heath, J.D. Morris³
H.H. Wills Physics Laboratory, University of Bristol, Bristol, United Kingdom^m

M. Kaur, P. Kaur⁴, I. Singh⁴
Panjab University, Department of Physics, Chandigarh, India

M. Capua, S. Fazio, A. Mastroberardino, M. Schioppa, G. Susinno, E. Tassi
Calabria University, Physics Department and INFN, Cosenza, Italy^e

J.Y. Kim
Chonnam National University, Kwangju, South Korea

Z.A. Ibrahim, F. Mohamad Idris, B. Kamaluddin, W.A.T. Wan Abdullah
Jabatan Fizik, Universiti Malaya, 50603 Kuala Lumpur, Malaysia^r

Y. Ning, Z. Ren, F. Sciulli
Nevis Laboratories, Columbia University, Irvington on Hudson, New York 10027, USA^o

J. Chwastowski, A. Eskreys, J. Figiel, A. Galas, K. Olkiewicz, B. Pawlik, P. Stopa,
L. Zawiejski
*The Henryk Niewodniczanski Institute of Nuclear Physics, Polish Academy of Sciences,
Cracow, Poland*ⁱ

L. Adamczyk, T. Bołd, I. Grabowska-Bołd, D. Kisielewska, J. Łukasik⁵, M. Przybycień,
L. Suszycki
*Faculty of Physics and Applied Computer Science, AGH-University of Science and Technology,
Cracow, Poland*^p

A. Kotański⁶, W. Słomiński⁷

Department of Physics, Jagellonian University, Cracow, Poland

O. Behnke, J. Behr, U. Behrens, C. Blohm, K. Borras, D. Bot, R. Ciesielski, N. Coppola, S. Fang, A. Geiser, P. Göttlicher⁸, J. Grebenyuk, I. Gregor, T. Haas, W. Hain, A. Hüttmann, F. Januschek, B. Kahle, I.I. Katkov⁹, U. Klein¹⁰, U. Kötz, H. Kowalski, M. Lisovyi, E. Lobodzinska, B. Lühr, R. Mankel¹¹, I.-A. Melzer-Pellmann, S. Miglioranza¹², A. Montanari, T. Namsoo, D. Notz, A. Parenti, P. Roloff, I. Rubinsky, U. Schneekloth, A. Spiridonov¹³, D. Szuba¹⁴, J. Szuba¹⁵, T. Theedt, J. Tomaszewska¹⁶, G. Wolf, K. Wrona, A.G. Yagües-Molina, C. Youngman, W. Zeuner¹¹

Deutsches Elektronen-Synchrotron DESY, Hamburg, Germany

V. Drugakov, W. Lohmann, S. Schlenstedt

Deutsches Elektronen-Synchrotron DESY, Zeuthen, Germany

G. Barbagli, E. Gallo

INFN Florence, Florence, Italy^e

P. G. Pelfer

University and INFN Florence, Florence, Italy^e

A. Bamberger, D. Dobur, F. Karstens, N.N. Vlasov¹⁷

Fakultät für Physik der Universität Freiburg i.Br., Freiburg i.Br., Germany^b

P.J. Bussey, A.T. Doyle, M. Forrest, D.H. Saxon, I.O. Skillicorn

Department of Physics and Astronomy, University of Glasgow, Glasgow, United Kingdom^m

I. Gialas¹⁸, K. Papageorgiu

Department of Engineering in Management and Finance, Univ. of Aegean, Greece

U. Holm, R. Klanner, E. Lohrmann, H. Perrey, P. Schleper, T. Schörner-Sadenius, J. Sztuk, H. Stadie, M. Turcato

Hamburg University, Institute of Exp. Physics, Hamburg, Germany^b

C. Foudas, C. Fry, K.R. Long, A.D. Tapper

Imperial College London, High Energy Nuclear Physics Group, London, United Kingdom^m

T. Matsumoto, K. Nagano, K. Tokushuku¹⁹, S. Yamada, Y. Yamazaki²⁰

Institute of Particle and Nuclear Studies, KEK, Tsukuba, Japan^f

A.N. Barakbaev, E.G. Boos, N.S. Pokrovskiy, B.O. Zhautykov

Institute of Physics and Technology of Ministry of Education and Science of Kazakhstan, Almaty, Kazakhstan

V. Aushev²¹, O. Bachynska, M. Borodin, I. Kadenko, O. Kuprash, V. Libov, D. Lon-
tkovskyi, I. Makarenko, Iu. Sorokin, A. Verbytskyi, O. Volynets, M. Zolko
*Institute for Nuclear Research, National Academy of Sciences, and Kiev National Univer-
sity, Kiev, Ukraine*

D. Son
Kyungpook National University, Center for High Energy Physics, Daegu, South Korea ^g

J. de Favereau, K. Piotrkowski
Institut de Physique Nucléaire, Université Catholique de Louvain, Louvain-la-Neuve, Belgium ^g

F. Barreiro, C. Glasman, M. Jimenez, J. del Peso, E. Ron, J. Terrón, C. Uribe-Estrada
Departamento de Física Teórica, Universidad Autónoma de Madrid, Madrid, Spain ^l

F. Corriveau, J. Schwartz, C. Zhou
Department of Physics, McGill University, Montréal, Québec, Canada H3A 2T8 ^a

T. Tsurugai
Meiji Gakuin University, Faculty of General Education, Yokohama, Japan ^f

A. Antonov, B.A. Dolgoshein, D. Gladkov, V. Sosnovtsev, A. Stifutkin, S. Suchkov
Moscow Engineering Physics Institute, Moscow, Russia ^j

R.K. Dementiev, P.F. Ermolov[†], L.K. Gladilin, Yu.A. Golubkov, L.A. Khein, I.A. Korzhavina,
V.A. Kuzmin, B.B. Levchenko²², O.Yu. Lukina, A.S. Proskuryakov, L.M. Shcheglova,
D.S. Zotkin
Moscow State University, Institute of Nuclear Physics, Moscow, Russia ^k

I. Abt, A. Caldwell, D. Kollar, B. Reiser, W.B. Schmidke
Max-Planck-Institut für Physik, München, Germany

G. Grigorescu, A. Keramidas, E. Koffeman, P. Kooijman, A. Pellegrino, H. Tiecke,
M. Vázquez¹², L. Wiggers
NIKHEF and University of Amsterdam, Amsterdam, Netherlands ^h

N. Brümmer, B. Bylsma, L.S. Durkin, A. Lee, T.Y. Ling
Physics Department, Ohio State University, Columbus, Ohio 43210, USA ⁿ

P.D. Allfrey, M.A. Bell, A.M. Cooper-Sarkar, R.C.E. Devenish, J. Ferrando, B. Foster,
C. Gwenlan²³, K. Horton²⁴, K. Oliver, A. Robertson, R. Walczak
Department of Physics, University of Oxford, Oxford United Kingdom ^m

A. Bertolin, F. Dal Corso, S. Dusini, A. Longhin, L. Stanco
INFN Padova, Padova, Italy ^e

R. Brugnera, R. Carlin, A. Garfagnini, S. Limentani
Dipartimento di Fisica dell' Università and INFN, Padova, Italy ^e

B.Y. Oh, A. Raval, J.J. Whitmore²⁵

*Department of Physics, Pennsylvania State University, University Park, Pennsylvania
16802^o*

Y. Iga

Polytechnic University, Sagamihara, Japan^f

G. D'Agostini, G. Marini, A. Nigro

Dipartimento di Fisica, Università 'La Sapienza' and INFN, Rome, Italy^e

J.E. Cole²⁶, J.C. Hart

Rutherford Appleton Laboratory, Chilton, Didcot, Oxon, United Kingdom^m

H. Abramowicz²⁷, R. Ingber, S. Kananov, A. Levy, A. Stern

*Raymond and Beverly Sackler Faculty of Exact Sciences, School of Physics, Tel Aviv
University,
Tel Aviv, Israel^d*

M. Kuze, J. Maeda

Department of Physics, Tokyo Institute of Technology, Tokyo, Japan^f

R. Hori, S. Kagawa²⁸, N. Okazaki, S. Shimizu, T. Tawara

Department of Physics, University of Tokyo, Tokyo, Japan^f

R. Hamatsu, H. Kaji²⁹, S. Kitamura³⁰, O. Ota³¹, Y.D. Ri

Tokyo Metropolitan University, Department of Physics, Tokyo, Japan^f

M. Costa, M.I. Ferrero, V. Monaco, R. Sacchi, V. Sola, A. Solano

Università di Torino and INFN, Torino, Italy^e

M. Arneodo, M. Ruspa

Università del Piemonte Orientale, Novara, and INFN, Torino, Italy^e

S. Fourletov³², J.F. Martin, T.P. Stewart

Department of Physics, University of Toronto, Toronto, Ontario, Canada M5S 1A7^a

S.K. Boutle¹⁸, J.M. Butterworth, T.W. Jones, J.H. Loizides, M. Wing³³

Physics and Astronomy Department, University College London, London, United Kingdom^m

B. Brzozowska, J. Ciborowski³⁴, G. Grzelak, P. Kulinski, P. Łuźniak³⁵, J. Malka³⁵, R.J. Nowak,
J.M. Pawlak, W. Perlanski³⁵, A.F. Żarnecki

Warsaw University, Institute of Experimental Physics, Warsaw, Poland

M. Adamus, P. Plucinski³⁶

Institute for Nuclear Studies, Warsaw, Poland

Y. Eisenberg, D. Hochman, U. Karshon

Department of Particle Physics, Weizmann Institute, Rehovot, Israel^c

E. Brownson, D.D. Reeder, A.A. Savin, W.H. Smith, H. Wolfe

Department of Physics, University of Wisconsin, Madison, Wisconsin 53706, USA ⁿ

S. Bhadra, C.D. Catterall, Y. Cui, G. Hartner, S. Menary, U. Noor, J. Standage, J. Whyte

Department of Physics, York University, Ontario, Canada M3J 1P3 ^a

- ¹ also affiliated with University College London, United Kingdom
- ² now at University of Salerno, Italy
- ³ now at Queen Mary University of London, UK
- ⁴ also working at Max Planck Institute, Munich, Germany
- ⁵ now at Institute of Aviation, Warsaw, Poland
- ⁶ supported by the research grant No. 1 P03B 04529 (2005-2008)
- ⁷ This work was supported in part by the Marie Curie Actions Transfer of Knowledge project COCOS (contract MTKD-CT-2004-517186)
- ⁸ now at DESY group FEB, Hamburg, Germany
- ⁹ also at Moscow State University, Russia
- ¹⁰ now at University of Liverpool, UK
- ¹¹ on leave of absence at CERN, Geneva, Switzerland
- ¹² now at CERN, Geneva, Switzerland
- ¹³ also at Institut of Theoretical and Experimental Physics, Moscow, Russia
- ¹⁴ also at INP, Cracow, Poland
- ¹⁵ also at FPACS, AGH-UST, Cracow, Poland
- ¹⁶ partially supported by Warsaw University, Poland
- ¹⁷ partly supported by Moscow State University, Russia
- ¹⁸ also affiliated with DESY, Germany
- ¹⁹ also at University of Tokyo, Japan
- ²⁰ now at Kobe University, Japan
- ²¹ supported by DESY, Germany
- ²² partly supported by Russian Foundation for Basic Research grant No. 05-02-39028-NSFC-a
- ²³ STFC Advanced Fellow
- ²⁴ nee Korcsak-Gorzo
- ²⁵ This material was based on work supported by the National Science Foundation, while working at the Foundation.
- ²⁶ now at University of Kansas, Lawrence, USA
- ²⁷ also at Max Planck Institute, Munich, Germany, Alexander von Humboldt Research Award
- ²⁸ now at KEK, Tsukuba, Japan
- ²⁹ now at Nagoya University, Japan
- ³⁰ member of Department of Radiological Science, Tokyo Metropolitan University, Japan
- ³¹ now at SunMelx Co. Ltd., Tokyo, Japan
- ³² now at University of Bonn, Germany
- ³³ also at Hamburg University, Inst. of Exp. Physics, Alexander von Humboldt Research Award and partially supported by DESY, Hamburg, Germany
- ³⁴ also at Łódź University, Poland
- ³⁵ member of Łódź University, Poland
- ³⁶ now at Lund University, Lund, Sweden
- † deceased

- a* supported by the Natural Sciences and Engineering Research Council of Canada (NSERC)
- b* supported by the German Federal Ministry for Education and Research (BMBF), under contract Nos. 05 HZ6PDA, 05 HZ6GUA, 05 HZ6VFA and 05 HZ4KHA
- c* supported in part by the MINERVA Gesellschaft für Forschung GmbH, the Israel Science Foundation (grant No. 293/02-11.2) and the US-Israel Binational Science Foundation
- d* supported by the Israel Science Foundation
- e* supported by the Italian National Institute for Nuclear Physics (INFN)
- f* supported by the Japanese Ministry of Education, Culture, Sports, Science and Technology (MEXT) and its grants for Scientific Research
- g* supported by the Korean Ministry of Education and Korea Science and Engineering Foundation
- h* supported by the Netherlands Foundation for Research on Matter (FOM)
- i* supported by the Polish State Committee for Scientific Research, project No. DESY/256/2006 - 154/DES/2006/03
- j* partially supported by the German Federal Ministry for Education and Research (BMBF)
- k* supported by RF Presidential grant N 1456.2008.2 for the leading scientific schools and by the Russian Ministry of Education and Science through its grant for Scientific Research on High Energy Physics
- l* supported by the Spanish Ministry of Education and Science through funds provided by CICYT
- m* supported by the Science and Technology Facilities Council, UK
- n* supported by the US Department of Energy
- o* supported by the US National Science Foundation. Any opinion, findings and conclusions or recommendations expressed in this material are those of the authors and do not necessarily reflect the views of the National Science Foundation.
- p* supported by the Polish Ministry of Science and Higher Education as a scientific project (2006-2008)
- q* supported by FNRS and its associated funds (IISN and FRIA) and by an Inter-University Attraction Poles Programme subsidised by the Belgian Federal Science Policy Office
- r* supported by an FRGS grant from the Malaysian government

1 Introduction

The formation of jets of hadrons can be described as a convolution of parton showering and hadronisation. Within perturbative QCD (pQCD), the parton shower can be described as long as the energy scale involved is sufficiently above the intrinsic scale of QCD, Λ_{QCD} . Hadronisation describes the process by which coloured partons become confined in colour-neutral hadrons. It cannot be described within pQCD.

Perturbative QCD calculations can be performed using matrix elements up to a certain order in the strong coupling constant, α_s . Alternatively, a resummation approach can be adopted, such as the modified leading-logarithmic approximation (MLLA) [1], where in addition to the fixed-order matrix elements, a subset of dominant terms of all orders in α_s are included. In particular, pQCD based on the MLLA can be used to predict the multiplicity and momentum spectra of partons produced within cones centred on the initial parton direction. The MLLA may only be used to describe partons at scales above some minimum cutoff, $\Lambda_{\text{eff}} > \Lambda_{\text{QCD}}$. The value of Λ_{eff} is predicted to be independent of the process considered. The local parton hadron duality (LPHD) [2] hypothesis predicts that charged-hadron distributions should be related to the predicted parton distributions by a constant normalisation scaling factor, κ^{ch} .

Tests of the MLLA have been performed before using data from e^+e^- collisions at LEP [3, 4] and PETRA [5], deep inelastic scattering (DIS) ep collisions at HERA [6, 7], (anti-)neutrino-nucleon interactions from the NOMAD experiment [8] and $p\bar{p}$ collisions at the Tevatron [9]. In this analysis, the multiplicity and momentum spectra of charged hadrons within jets are studied using photoproduction (γp) in ep collisions, in which a quasi-real photon emitted from the incoming electron collides with a proton. The events were required to have two and only two reconstructed jets and the sample was enriched in events in which the photon interacted electromagnetically as a point-like particle. The analysis probes energy scales in the range 19 to 38 GeV, which spans the energy region between those accessed previously by the ZEUS, using ep DIS collisions [6, 7], and CDF collaborations [9]. The quantities Λ_{eff} and κ^{ch} are extracted and their universality tested.

2 The MLLA framework

The MLLA includes all terms of order $\alpha_s^n \log^{2n}(E_{\text{init}}^{\text{pl}})$ and $\alpha_s^n \log^{2n-1}(E_{\text{init}}^{\text{pl}})$, where n is the set of positive integers and $E_{\text{init}}^{\text{pl}}$ is the energy of the initial outgoing parton in the centre-of-mass frame of the incoming struck parton and exchanged photon. The “pl” superscript denotes a parton-level quantity. The MLLA accounts for colour-coherence effects between diagrams of the same order of α_s by enforcing an angular-ordering scheme [10].

The MLLA equations describe the momentum and multiplicity spectra of partons at a specified scale, Q_0 . They are only strictly valid for partons satisfying $x_p^{\text{pl}} = |p_p^{\text{pl}}|/E_{\text{init}}^{\text{pl}} \ll 1$, where p_p^{pl} is the 3-momentum of a parton in the centre-of-mass frame. For the MLLA predictions used here, the singularities were regularised by a single $p_T^{\text{rel,pl}}$ cut-off at scale $Q_0 > \Lambda_{\text{eff}}$, where $p_T^{\text{rel,pl}}$ is the transverse momentum with which the parton was emitted with respect to its parent. This is not the only possible way to regularise the MLLA; other forms lead to different predictions, particularly at low x_p^{pl} [11].

Predictions at the lowest valid scale, $Q_0 = \Lambda_{\text{eff}}$, give the so-called limiting momentum spectrum of partons, $\bar{D}^{\text{lim,pl}} = \frac{dN^{\text{pl}}}{d\xi^{\text{pl}}}$, where $\xi^{\text{pl}} = \ln(1/x_p^{\text{pl}})$ and N^{pl} is the multiplicity of partons produced within a cone of opening angle, θ_c^{pl} , measured with respect to the axis of the initial parton. The predictions assume that θ_c^{pl} is small. The shape of the predicted spectrum is roughly Gaussian, although it falls rapidly to zero as $\xi^{\text{pl}} \rightarrow \ln\left(E_{\text{init}}^{\text{pl}} \sin(\theta_c^{\text{pl}})/\Lambda_{\text{eff}}\right)$, a consequence of the regularisation scheme adopted.

For a gluon-initiated parton-level jet, the function is written as [12]

$$\bar{D}_{\text{g-jet}}^{\text{lim,pl}} = F_{\text{nMLLA}} \frac{4n_c}{b} \Gamma(B) \int_{-\pi/2}^{\pi/2} e^{-B\alpha} \left[\frac{\cosh \alpha + (1 - 2\zeta) \sinh \alpha}{\frac{4n_c}{b} Y \frac{\alpha}{\sinh \alpha}} \right]^{B/2} I_B \left(\sqrt{\frac{16n_c}{b} Y \frac{\alpha}{\sinh \alpha} [\cosh \alpha + (1 - 2\zeta) \sinh \alpha]} \right) \frac{d\tau}{\pi}, \quad (1)$$

where the parameters $b = 9$ and $B = 101/81$ are QCD constants defined in terms of the number of colours, $n_c = 3$, and number of flavours, $n_f = 3$. The symbols Γ and I_B denote the Gamma and B^{th} -order modified Bessel functions, respectively. The other variables are defined as

$$Y = \ln(E_{\text{init}}^{\text{pl}} \sin(\theta_c^{\text{pl}})/\Lambda_{\text{eff}}), \quad \zeta = 1 - \xi^{\text{pl}}/Y, \quad \alpha = \tanh^{-1}(2\zeta - 1) + i\tau, \quad (2)$$

and, in the MLLA, $F_{\text{nMLLA}} = 1$. The value of $n_f = 3$ was chosen. The MLLA assumes massless partons and does not include any mass threshold effects for heavy flavours. When a value of n_f larger than 3 is used instead, the theory is observed to give a poorer description of this and other data sets [12].

At leading order (LO), the peak position of the limiting momentum spectrum, $\xi_{\text{peak}}^{\text{pl}}$, is predicted to be at

$$\xi_{\text{peak}}^{\text{pl}} = \frac{1}{2}Y + \sqrt{cY} - c, \quad (3)$$

where $c = 0.29$.

The limiting spectrum of quark jets, $\bar{D}_{\text{q-jet}}^{\text{lim,pl}}$, is related to that of gluon jets according to

$$\bar{D}_{\text{q-jet}}^{\text{lim,pl}} = \frac{1}{r} \bar{D}_{\text{g-jet}}^{\text{lim,pl}}, \quad (4)$$

where $r = N_{g\text{-jet}}^{\text{pl}}/N_{q\text{-jet}}^{\text{pl}}$ is the ratio of parton multiplicities in gluon- and quark-initiated jets. In the MLLA, $r = C_A/C_F = 9/4$ where C_A and C_F are the gluon and quark colour factors, respectively.

Photoproduction samples contain both gluon- and quark-initiated jets, in the fractions denoted by ϵ_g and $\epsilon_q = 1 - \epsilon_g$, respectively. Thus, the limiting spectrum for partons in all jets can be parameterised as

$$\bar{D}^{\text{lim,pl}} = \left(\epsilon_g + \frac{1 - \epsilon_g}{r} \right) \bar{D}_{g\text{-jet}}^{\text{lim,pl}}. \quad (5)$$

Solutions to the MLLA evolution equations have also been made at so-called next-to-MLLA order. Each of these solutions partially accounts for orders not included in the equations above. With the next-to-MLLA corrections, F_{nMLLA} and r differ from their MLLA values and both have a weak dependence on $E_{\text{init}}^{\text{pl}}$. Next-to-MLLA F_{nMLLA} and r values have been used in this analysis in the same way as they were by the CDF collaboration [9], wherein more details can be found. Their values were taken from three different next-to-MLLA calculations [13], which differ in the way the additional orders are accounted for, leading to some spread in the predicted F_{nMLLA} and r values. Here, constant values of $F_{\text{nMLLA}} = 1.3 \pm 0.2$ and $r = 1.6 \pm 0.2$ were used, with the theoretical uncertainties covering the spreads.

The LPHD approximation relates the limiting momentum spectrum of partons to that of charged hadrons within jets, $\bar{D}^{\text{lim,ch}}$, via

$$\bar{D}^{\text{lim,ch}} = \kappa^{\text{ch}} \bar{D}^{\text{lim,pl}} = \kappa^{\text{ch}} \left(\epsilon_g + \frac{1 - \epsilon_g}{r} \right) \bar{D}_{g\text{-jet}}^{\text{lim,pl}} = K \bar{D}_{g\text{-jet}}^{\text{lim,pl}}, \quad (6)$$

i.e. $K = \kappa^{\text{ch}} (\epsilon_g + (1 - \epsilon_g)/r)$. Due to isospin invariance, κ^{ch} is expected to be approximately $2/3$.

3 The analysis strategy

To compare the parton-level MLLA predictions to measured hadron-level data, while assuming LPHD, each variable within the MLLA had to be estimated using a related hadron-level quantity. The hadron-level estimator for $E_{\text{init}}^{\text{pl}}$ was chosen to be $E_{\text{jet}} = M_{2j}/2$, where E_{jet} is the energy of either hadron-level jet in the dijet centre-of-mass frame and M_{2j} is the invariant dijet mass. The quantity p_p^{pl} was estimated using the momenta of the charged hadrons, p_{trk} . The loss of the neutral hadrons is accounted for via the LPHD factor κ^{ch} . The MLLA variable θ_c^{pl} was estimated using the opening angle of a cone measured with respect to the reconstructed jet axis, θ_c . Accordingly, the quantity $\bar{D}^{\text{lim,ch}}$,

given in Eq. 6, was estimated using the hadron-level multiplicity distribution of charged hadrons per jet, $N_{\text{jet}}^{\text{ch}}$, measured in bins of E_{jet} and in cones of varying θ_c , differentially in $\xi = \ln(E_{\text{jet}}/|p_{\text{trk}}|)$. These $dN_{\text{jet}}^{\text{ch}}/d\xi$ distributions will be referred to as the ξ distributions.

4 Experimental setup

The data analysed here were collected using the ZEUS detector during the 2005 to 2007 running periods, in which electrons¹ were collided with protons with energies of $E_e = 27.5$ GeV and $E_p = 920$ GeV, respectively, corresponding to a centre-of-mass energy, $\sqrt{s} = 318$ GeV. The total sample corresponds to an integrated luminosity of 359 ± 9 pb⁻¹. A detailed description of the ZEUS detector can be found elsewhere [14, 15]. A brief outline of the components most relevant to this analysis is given below.

Charged particles were tracked in the central tracking detector (CTD) [16], the microvertex detector (MVD) [17] and the straw-tube tracker (STT) [18]. The CTD and MVD were operated in a magnetic field of 1.43 T provided by a thin superconducting solenoid. The CTD drift chamber covered the polar-angle² region $15^\circ < \theta < 164^\circ$. The MVD silicon tracker consisted of a barrel (BMVD) and a forward (FMVD) section. The BMVD provided polar-angle coverage for tracks with three measurements from 30° to 150° . The FMVD extended the polar-angle coverage in the forward region to 7° . The STT covered the polar-angle region $5^\circ < \theta < 25^\circ$.

The high-resolution uranium-scintillator calorimeter (CAL) [19] consisted of three parts: the forward, the barrel and the rear calorimeters. Each part was subdivided transversely into towers and longitudinally into one electromagnetic and either one (in the rear) or two (in the barrel and forward) hadronic sections. The smallest subdivision of the calorimeter was called a cell. The CAL relative energy resolutions, as measured under test-beam conditions, were $0.18/\sqrt{E}$ for electrons and $0.35/\sqrt{E}$ for hadrons, with E in GeV.

5 Event reconstruction

A three-level trigger system was used to select events online [15, 20, 21]. At the first two levels, general characteristics of photoproduction collisions were required and background

¹ The word “electron” is used as a generic term for electrons and positrons.

² The ZEUS coordinate system is a right-handed Cartesian system, with the Z axis pointing in the proton beam direction, referred to as the “forward direction”, and the X axis pointing towards the centre of HERA. The coordinate origin is at the nominal interaction point.

from beam-gas events was rejected. At the third level, jets were reconstructed by applying the k_T cluster algorithm [22] to the CAL cells and a loose dijet selection was applied.

In the offline analysis, the hadronic final state was reconstructed using energy-flow objects [23, 24] (EFOs), which were formed from a combination of track and calorimeter information. This approach optimised the energy resolution and improved the one-to-one correspondence between the detector-level objects and the hadrons. The EFOs were corrected to account for energy losses in the dead material and were forced to be massless by setting the energy component equal to the magnitude of the three-momentum.

Jets were reconstructed from EFOs using the k_T cluster algorithm [22] in the longitudinally invariant inclusive mode [25] using the p_T recombination scheme and with the R parameter set to $R = 1$.

Photoproduction events are characterised by the low virtuality, Q^2 , of the exchanged photon. At LO, photoproduction can be categorised as being either direct, if the photon interacts as a point-like particle, or resolved, if it fluctuates into a partonic system, which then interacts with the proton. The LO direct photoproduction processes are boson gluon fusion, $\gamma g \rightarrow q\bar{q}$, and QCD Compton scattering, $\gamma q \rightarrow qg$. Important kinematic variables are the inelasticity, y , and the fraction of the photon momentum transferred to the hadronic final state, x_γ . The variable x_γ can be approximated using the observable x_γ^{obs} , defined for a dijet event as

$$x_\gamma^{\text{obs}} = \frac{\sum_{i=1}^2 E_T^{\text{jet}(i)} \exp(-\eta^{\text{jet}(i)})}{2yE_e}, \quad (7)$$

where E_T^{jet} and η^{jet} denote the jet transverse energy and pseudorapidity in the laboratory frame, respectively. A value of x_γ^{obs} approaching one indicates an event from a direct-like photoproduction process.

6 Event selection

To remove non-photoproduction events it was required that:

- the longitudinal position of the reconstructed vertex was in the range $|Z_{\text{vtx}}| \leq 40$ cm;
- $0.2 \leq y_{\text{JB}} \leq 0.85$, where y_{JB} is the Jacquet–Blondel estimator [26] of y ;
- no scattered electron was observed in the CAL with $E'_e > 5$ GeV and $y_e < 0.85$, where E'_e is the energy of the scattered electron and y_e is the electron-method estimator of y [27];
- $P_T^{\text{miss}}/\sqrt{E_T} \leq 2$ GeV^{1/2}, where P_T^{miss} and E_T are the reconstructed missing and total transverse momenta, respectively;

- $|t_{\text{CAL}}^{\text{top}} - t_{\text{CAL}}^{\text{bot}}| < 6$ ns, where $|t_{\text{CAL}}^{\text{top}} - t_{\text{CAL}}^{\text{bot}}|$ is the difference between the arrival times of the first signals in the top and bottom halves of the CAL;
- $N_{\text{trk}}^{\text{pri}}/N_{\text{trk}} > 0.1$, where $N_{\text{trk}}^{\text{pri}}/N_{\text{trk}}$ is the ratio of the number of tracks fitted to the primary vertex to the total number of all tracks.

To select an exclusive dijet sample enriched in direct events it was required that:

- two jets were found such that:
 - the highest E_T^{jet} jet, labelled 1, had $|\eta^{\text{jet1}}| \leq 1$ and $E_T^{\text{jet1}} \geq 17$ GeV;
 - the second jet, labelled 2, had $|\eta^{\text{jet2}}| \leq 1$ and $E_T^{\text{jet2}}/E_T^{\text{jet1}} \geq 0.8$;
 - the first and second jets satisfied $|\phi^{\text{jet1}} - \phi^{\text{jet2}}| \geq 0.9\pi$, where ϕ^{jet} denotes the azimuthal angle of the jet;
- no third jet was found with $|\eta^{\text{jet3}}| \leq 2.4$ and $E_T^{\text{jet3}} \geq 6$ GeV;
- $x_\gamma^{\text{obs}} \geq 0.75$.

To ensure that the tracks were well reconstructed and not associated with secondary charged particles generated via nuclear interactions within the detector material it was required that:

- the track transverse momentum was greater than 150 MeV;
- the track pseudorapidity was between ± 1.7 ;
- the track passed through at least 3 CTD super layers;
- the track was associated to the primary vertex.

The requirement that there be two and only two jets roughly balancing in E_T^{jet} and in opposite hemispheres ensured that the events were LO-like, where the energy scale is well estimated using $M_{2j}/2$. The x_γ^{obs} criterion was applied to minimise the influence of multi-parton interactions (MPIs) [28–30], which generate additional final-state hadrons and can disrupt the correspondence between the MLLA predictions and the data. After all the above selection, the data sample contained 23,449 events.

7 Acceptance corrections

Effects due to the limited detector and trigger acceptance, efficiency and resolution were corrected for in the data using a sample of events generated with the PYTHIA MC model [31]. The direct and resolved photoproduction processes were generated separately and combined in the ratio that best fit the x_γ^{obs} distribution in the data. The PYTHIA model includes the LO ($2 \rightarrow 2$) matrix elements, approximates higher-order processes

using initial-state and final-state parton showers and simulates hadronisation using the Lund string model [32]. The CTEQ5L [33] and GRV-G LO [34] parameterisations were used to describe the proton and photon PDFs, respectively. The main sample included MPIs, simulated using the “simple model” [31] within PYTHIA, although the effects from MPIs were predicted to be negligible in the final sample. The detector simulation was based on GEANT 3.21 [35] and included a complete simulation of the three-level trigger system.

The data were corrected bin-by-bin to the hadron-level using factors extracted from the MC equal to the ratio of the predicted hadron- to detector-level cross sections. Here, the hadron-level was defined to contain all particles with an average lifetime greater than 0.01 ns. The size of the bin-by-bin corrections were typically around 1.5.

The normalisation of the ξ distributions was set such that the integral of the distributions over the full ξ range equalled $\langle N_{\text{jet}}^{\text{ch}} \rangle$, where $\langle N_{\text{jet}}^{\text{ch}} \rangle$ denotes the average hadron-level charged-particle multiplicity within jets, with the appropriate cone and energy scale criteria applied. The values of $\langle N_{\text{jet}}^{\text{ch}} \rangle$ were extracted from the data by measuring the corresponding charged multiplicity distributions. These were corrected to the hadron-level using unfolding matrices derived from the PYTHIA MC sample. Full details of the procedure are described elsewhere [6, 36].

8 Systematic uncertainties

A detailed study [37] of the sources of systematic uncertainty associated with the measurement was performed. The dominant sources contributing to the systematic uncertainty on the ξ distributions are listed below (the numbers in parentheses refer to the maximum uncertainty observed in any one bin):

- the $\pm 3\%$ uncertainty in the CAL energy scale, propagated to the ξ distributions by varying the CAL energies in the MC simulation accordingly ($\pm 4\%$);
- the uncertainty simulating nuclear interactions in the detector material and the production of charged secondary particles. This was propagated to the ξ distributions by varying the difference between the number of tracks gained and lost due to such effects in the MC by a factor of 2 ($\pm 4\%$);
- the uncertainty in the tracking efficiency, propagated to the ξ distributions using the procedure described below (+5%).

The MC slightly overestimated the number of tracks in the data, probably due to either the uncertainty in the hadronisation model or to inadequacies in the detector simulation. The unfolding procedure is only strongly sensitive to the detector-level simulation rather

than the hadron-level MC model and it was assumed that this was the sole cause of the excess. This systematic uncertainty was evaluated by randomly failing detector-level tracks in the MC with track rejection rates evaluated in bins of E_{jet} , θ_{trk} and $1/p_{\text{trk}}$, where θ_{trk} is the polar angle between the track and the jet axis. The largest rejection rate was 14%. The analysis was then repeated and the resulting difference in the ξ distributions was included in the systematic uncertainty. All the systematic uncertainties were added in quadrature.

In the next section, several fits of the data are discussed. While nominally fitting the data and when evaluating the associated χ^2 values, only the statistical uncertainties were considered. The systematic uncertainties on the data were propagated, however, to the fitted parameters using the “offset method”. To apply the “offset method”, the fit is repeated for each source of systematic uncertainty, shifting the nominal data by the uncertainty attributed to that one source. The differences between the values of the parameters extracted from the nominal and the shifted data are then summed in quadrature and included as the total systematic uncertainty on the parameter itself.

9 Results and discussion

The ξ distributions were measured in five bins of E_{jet} and in cones around the reconstructed jet axes with opening angles $\theta_c = \{0.23, 0.28, 0.34\}$. The characteristic energy scales of the five E_{jet} bins, $E_{\text{jet}} = \{19, 23, 28, 32, 38\}$ GeV, were equated with the mean E_{jet} value for all events contributing to that bin. They are shown in Fig. 1. Each of the distributions are observed to be similar in shape and are roughly Gaussian with more pronounced upper tails.

To assess the validity of the MLLA predictions using the measured ξ distributions, two approaches were adopted. The first, discussed in Section 9.1, was based solely on the position of the peak of the ξ distributions, ξ_{peak} . The second was based on the full shape of the ξ distributions and is discussed in Section 9.2.

9.1 The ξ_{peak} analysis

The values of ξ_{peak} were extracted from the ξ distributions using a three-parameter Gaussian fit. In accordance with previous analyses [6, 9], the distributions were fit in the range $\mu_\xi \pm 1$, where μ_ξ is the arithmetic mean of the ξ distribution over the full ξ range. The explicit ranges and χ^2/dof values of the fits are given in Fig. 1. The χ^2/dof values range between 0.48 and 1.33 and hence indicate that the fits are reasonable.

Uncertainty in the ξ_{peak} values due to the choice of fitting range was added in quadrature to the total systematic uncertainty. It was evaluated by changing the fit range to $\mu_\xi \pm 0.9$ and $\mu_\xi \pm 1.1$, leading maximally to a ${}^{+0.14}_{-1.31}\%$ systematic effect. The largest and only other source contributing more than 1% to the systematic uncertainty was the CAL energy scale, leading to a ${}^{+0.58}_{-2.86}\%$ effect. The extracted values of ξ_{peak} are given in Table 1 and are observed to increase as the energy scale or θ_c increases.

The ξ_{peak} values are shown in Fig. 2 as a function of $\mu \sin(\theta_c)$, where the characteristic energy scale here is $\mu = E_{\text{jet}}$. Also shown at their characteristic energy scales are data from the ZEUS ep DIS [6, 9] analysis and the OPAL [3], TASSO [5], NOMAD [8] and CDF [9] collaborations. There is an approximately linear relationship between ξ_{peak} and $\ln(E_{\text{jet}} \sin(\theta_c))$. This relationship was tested by fitting the ξ_{peak} data, measured with $\theta_c = 0.23$, with a straight line, parameterised as $\xi_{\text{peak}} = A(\ln(E_{\text{jet}} \sin(\theta_c))) + B$. In the case where only the new ZEUS γp data were considered, the best fit values for the coefficients were found to be $A = 0.56 \pm 0.06(\text{stat.}) {}^{+0.08}_{-0.03}(\text{syst.})$ and $B = 1.16 \pm 0.09(\text{stat.}) {}^{+0.06}_{-0.14}(\text{syst.})$. The χ^2/dof of the fit was 0.51.

A test of the same linear relationship was made using the global data set in Fig. 2. The best global fit values for the coefficients were found to be $A = 0.682 \pm 0.007(\text{stat.} \oplus \text{syst.})$ and $B = 1.009 \pm 0.019(\text{stat.} \oplus \text{syst.})$, with a χ^2/dof of 0.77. Here, all systematic uncertainties were treated as uncorrelated. The globally-extracted parameters are consistent with those extracted from the ZEUS data alone. The ZEUS γp points are systematically below the global-fit line, however the differences are within the total experimental uncertainty.

The MLLA in fact predicts a small square-root correction to the perfect linear dependence, as seen in Eq. 3. Assuming Λ_{eff} is constant within the range of energies probed, Eq. 3 can be directly fit to the ξ_{peak} data, treating Λ_{eff} as a free parameter. In the case where only the ZEUS γp data with $\theta_c = 0.23$ were considered, the best fit value was found to be $\Lambda_{\text{eff}} = 275 \pm 4(\text{stat.}) {}^{+4}_{-8}(\text{syst.}) \text{ MeV}$. The χ^2/dof of the fit was 0.70, indicating a good fit. When the global data set was considered, the best fit value was found to be $\Lambda_{\text{eff}} = 246 \pm 3(\text{stat.} \oplus \text{syst.}) \text{ MeV}$. In the global fit, all uncertainties were treated as uncorrelated. The χ^2/dof of the fit, with this simplistic error treatment, was 2.2, indicating some discrepancy. The globally extracted value of Λ_{eff} is not consistent with that extracted from the ZEUS data alone.

The energy dependence of Λ_{eff} was studied by using Eq. 3 to map each ξ_{peak} value to a corresponding value of Λ_{eff} . The results, given in Table 2 and shown in Fig. 3 as a function of E_{jet} , show no evidence that Λ_{eff} is dependent on the energy scale. A weak dependence was observed in the CDF data [9], which span a wider range of energy scales. However, the data do suggest that the value of Λ_{eff} is weakly dependent on θ_c . Specifically, Fig. 3 shows that the values of Λ_{eff} extracted from the wider cone data tend to be systematically larger. This behaviour was also observed by the CDF collaboration [9]. Both the θ_c and

E_{jet} dependence seen by CDF would contribute to the discrepancy observed when fitting Eq. 3 to the global data set.

In Fig. 4, the values of Λ_{eff} extracted using the ξ_{peak} data are shown as a function of the energy scale and compared to the previous results from ZEUS [6] using ep DIS collisions, and the OPAL [3], L3 [4] and CDF [9] collaborations. The values are all largely consistent in the energy scale region shown, supporting the prediction that Λ_{eff} is a universal parameter.

9.2 The ξ -shape analysis

The ξ distributions were also fitted using the predicted limiting spectrum, according to Eq. 6. The quantities K and Λ_{eff} were treated as free parameters during the fit. The fitted MLLA functions are shown in Fig. 5. The fits were restricted to the ranges indicated by the vertical lines and the χ^2/dof values of the fits are also given and lie between 0.34 and 2.72. Typically, in each E_{jet} bin, the χ^2/dof increases as θ_c does. The χ^2/dof values indicate that, while the theory does describe many of the features of the data in the fitting ranges, there are differences. Specifically, the rising edges of the ξ peaks are well described. However, the upper tails of the distributions are not adequately reproduced. The same was observed in e^+e^- [3,4] and ep DIS [6] data and to a lesser extent in high- E_{jet} $p\bar{p}$ data [9]. This is likely due to the specific MLLA regularisation scheme used here and in the other aforementioned analyses.

As discussed in Section 2, the MLLA regularisation scheme used here causes the partons to be cut-off at $p_T^{\text{rel,pl}} = \Lambda_{\text{eff}}$, whereas the hadrons in the data are not. This leads to an intrinsic discrepancy between data and theory. The discrepancy is present for all $\xi > 0$, however the magnitude of the effect is small at low ξ and increases until, for all $\xi > \ln(E_{\text{jet}} \sin(\theta_c)/\Lambda_{\text{eff}})$, there are only hadrons and no partons.

A consequence of this discrepancy is that, in order to fit the data using Eq. 6, a relatively arbitrary upper fitting bound, ξ_+ , had to be chosen for each ξ distribution. The criteria used to set ξ_+ were that the resulting fits were reasonably stable and that $\xi_{\text{peak}} \ll \xi_+ < \ln(E_{\text{jet}}/250 \text{ MeV})$ was satisfied, where 250 MeV roughly corresponds to the values of Λ_{eff} extracted from the ξ_{peak} data. The finite experimental ξ binning was also a consideration. It was chosen to use $\xi_+ = w\xi_{\text{peak}} + (1-w)\ln(E_{\text{jet}}/250 \text{ MeV})$, with $w = 0.25$ for the nominal fits. The sensitivity of K and Λ_{eff} to the choice of the fitting range was treated as a systematic uncertainty and was evaluated by varying w by ± 0.1 . This source of uncertainty strongly dominates the overall uncertainty on Λ_{eff} , leading to a ${}^{+1.8}_{-10.6}\%$ effect, although K was found to be largely insensitive to it. The same lower fitting bound, $\xi_- = \ln(2)$, was used in all cases and both K and Λ_{eff} were observed to be insensitive to a variation of ξ_- by $\pm 15\%$.

The values of Λ_{eff} extracted from the MLLA fits are given in Table 2. The results are in reasonable agreement with those extracted from the ξ_{peak} data, although the values extracted using the MLLA fit have larger uncertainties. The value of Λ_{eff} from the MLLA method with $\theta_c = 0.23$ and averaged over E_{jet} , weighting each data point based only on its statistical precision, is $\Lambda_{\text{eff}} = 304 \pm 6(\text{stat.})_{-32}^{+8}(\text{syst.}) \text{ MeV}$.

Values of κ_{ch} were extracted from the fitted K values using Eq. 6 and the values of ϵ_g predicted for each E_{jet} bin by the PYTHIA model. The ϵ_g values were roughly constant in E_{jet} , at $\epsilon_g \approx 0.2$. The κ_{ch} values are given in Table 3 and are shown in Fig. 6. The total uncertainty is dominated by the theoretical uncertainty associated with the next-to-MLLA correction factors. The κ_{ch} data suggest a weak dependence on θ_c . Specifically, as θ_c increases, so too does the central value of κ_{ch} . This is significant when the high degree of statistical correlation between the three θ_c samples and the bin-to-bin correlation in the systematic and theoretical uncertainties are taken into consideration. The same is true for the κ_{ch} values reported by the CDF collaboration [9], which were obtained using a different extraction method. The ZEUS data in Fig. 6 do not provide any evidence that κ_{ch} is dependent on E_{jet} in the range probed.

The value of κ_{ch} , measured with $\theta_c = 0.23$ and averaged over E_{jet} , weighting the data points based on their statistical precision, was $\kappa_{\text{ch}} = 0.55 \pm 0.01(\text{stat.})_{-0.02}^{+0.03}(\text{syst.})_{-0.09}^{+0.11}(\text{theo.})$. The κ_{ch} value extracted here is in good agreement with that reported by the CDF collaboration, $\kappa_{\text{ch}} = 0.56 \pm 0.05(\text{stat.}) \pm 0.09(\text{syst.})$. To compare to the values extracted using e^+e^- and ep DIS data and assuming no contamination from gluon jets, the values have to be scaled by $rC_F/F_{\text{nMLLA}}C_A \approx 0.55$. This leads to values of $\kappa_{\text{ch}} \approx 0.7$. These other results were found with θ_c effectively set to $\pi/2$ however.

10 Summary

The multiplicity distributions of charged particles within cones centred on jets have been measured as a function of $\xi = \ln(1/x_p)$, where x_p is the fraction of the jet's momentum carried by the charged particle. These ξ distributions have been measured in five bins of E_{jet} and with three different cone opening angles, θ_c , for γp events containing two and only two jets, using 359 pb^{-1} of ep data.

The peak positions of the ξ distributions, ξ_{peak} , were extracted and observed to increase roughly linearly with $\ln(E_{\text{jet}} \sin(\theta_c))$. A single value of intrinsic MLLA scale, Λ_{eff} , was extracted by fitting the ξ_{peak} data according to the predicted relationship between ξ_{peak} and $\ln(E_{\text{jet}} \sin(\theta_c) / \Lambda_{\text{eff}})$. The best fit value was found to be $\Lambda_{\text{eff}} = 275 \pm 4(\text{stat.})_{-8}^{+4}(\text{syst.}) \text{ MeV}$.

The E_{jet} and θ_c dependences of Λ_{eff} were studied by calculating a value of Λ_{eff} from each ξ_{peak} data point. The value of Λ_{eff} weakly depends on θ_c but no E_{jet} dependence was

observed. The Λ_{eff} data are consistent with previously published data sets using different initial states, supporting the prediction that Λ_{eff} is universal.

The ξ distributions were also fitted using the limited momentum spectra predicted by the MLLA and assuming LPHD, in the regions where they are applicable. The theory largely described the data in these regions. The fitted MLLA functions were used to extract the value of Λ_{eff} as a function of E_{jet} and θ_c . The value extracted using this method with $\theta_c = 0.23$ and averaged over E_{jet} , was $\Lambda_{\text{eff}} = 304 \pm 6(\text{stat.})_{-32}^{+8}(\text{syst.})$ MeV.

The value of the LPHD parameter κ_{ch} was extracted as a function of E_{jet} and θ_c from the fitted limited momentum spectra. Corrections based on next-to-MLLA theory were included. The value extracted with $\theta_c = 0.23$ and averaged over E_{jet} , was $\kappa_{\text{ch}} = 0.55 \pm 0.01(\text{stat.})_{-0.02}^{+0.03}(\text{syst.})_{-0.09}^{+0.11}(\text{theo.})$. The value of κ_{ch} has a weak dependence on θ_c and is consistent with the results published by the CDF collaboration. The data support the assumption that κ_{ch} is universal.

11 Acknowledgments

We would like to sincerely thank Wolfgang Ochs for many highly illuminating conversations. We appreciate the contributions to the construction and maintenance of the ZEUS detector of many people who are not listed as authors. The HERA machine group and the DESY computing staff are especially acknowledged for their success in providing excellent operation of the collider and the data analysis environment. We thank the DESY directorate for their strong support and encouragement.

References

- [1] Y.L. Dokshitzer, V.S. Fadin and V.A. Khoze, Phys. Lett. **B 115**, 242 (1982);
A.H. Mueller, Nucl. Phys. **B 228**, 351 (1983);
A.H. Mueller, Nucl. Phys. **B 241**, 141 (1984);
E.D. Malaza and B.R. Webber, Phys. Lett. **B 149**, 501 (1984);
Y.L. Dokshitzer et al., *Basics of Perturbative QCD*. Editions Frontières, 1991;
Y.L. Dokshitzer, V.A. Khoze and S.I. Troian, Z. Phys. **C 55**, 107 (1992).
- [2] Y.I. Azimov et. al, Z. Phys. **C 27**, 65 (1985).
- [3] OPAL Coll., M.Z. Akrawy et al., Phys. Lett. **B 247**, 617 (1990).
- [4] L3 Coll., B. Adeva et al., Phys. Lett. **B 259**, 199 (1991).
- [5] TASSO Coll., W. Braunschweig et al., Z. Phys. **C 47**, 187 (1990).
- [6] ZEUS Coll., M. Derrick et al., Z. Phys. **C 67**, 93 (1995).
- [7] ZEUS Coll., J. Breitweg et al., Eur. Phys. J. **C 11**, 251 (1999).
- [8] NOMAD Coll., J. Altegoer et al., Phys. Lett. **B 445**, 439 (1999).
- [9] CDF Coll., D. Acosta et al., Phys. Rev. **D 68**, 012003 (2003).
- [10] B.I. Ermolaev and V.S. Fadin, JETP Lett. **33**, 269 (1981).
- [11] S. Lupia and W. Ochs, Eur. Phys. J. **C 2**, 307 (1998).
- [12] V.A. Khoze, W. Ochs and J. Wosiek, arXiv:hep-ph/0009298.
- [13] S. Lupia and W. Ochs, Phys. Lett. **B 418**, 214 (1998);
I.M. Dremin and J.W. Gary, Phys. Lett. **B 459**, 341 (1999);
S. Catani et al., Nucl. Phys. **B 383**, 419 (1992).
- [14] ZEUS Coll., M. Derrick et al., Phys. Lett. **B 297**, 404 (1992).
- [15] ZEUS Coll., U. Holm (ed.), *The ZEUS Detector*. Status Report (unpublished),
DESY (1993), available on <http://www-zeus.desy.de/bluebook/bluebook.html>.
- [16] N. Harnew et al., Nucl. Inst. Meth. **A 279**, 290 (1989);
B. Foster et al., Nucl. Phys. Proc. Suppl. **B 32**, 181 (1993);
B. Foster et al., Nucl. Inst. Meth. **A 338**, 254 (1994).
- [17] A. Polini et al., Nucl. Inst. Meth. **A 581**, 656 (2007).
- [18] S. Fourletov [ZEUS STT Collaboration], Nucl. Inst. Meth. **A 535**, 191 (2004).
- [19] M. Derrick et al., Nucl. Inst. Meth. **A 309**, 77 (1991);
A. Andresen et al., Nucl. Inst. Meth. **A 309**, 101 (1991);
A. Bernstein et al., Nucl. Inst. Meth. **A 336**, 23 (1993);
A. Caldwell et al., Nucl. Inst. Meth. **A 321**, 356 (1992).

- [20] ZEUS Coll., J. Breitweg et al., *Eur. Phys. J. C* **1**, 109 (1998).
- [21] W.H. Smith, K. Tokushuku and L.W. Wiggers, *Proc. Computing in High-Energy Physics (CHEP), Annecy, France*, C. Verkerk and W. Wojcik (eds.), p. 222. CERN, Geneva, Switzerland (1992). Also in preprint DESY 92-150B.
- [22] S. Catani et al., *Nucl. Phys. B* **406**, 187 (1993).
- [23] ZEUS Coll., J. Brietweg et al., *Eur. Phys. J. C* **6**, 43 (1999).
- [24] G.M. Briskin, Ph.D. Thesis, Tel Aviv University, Israel, 1998, DESY-THESIS-1998-036.
- [25] S.D. Ellis and D.E. Soper, *Phys. Rev. D* **48**, 3160 (1993).
- [26] F. Jacquet and A. Blondel, *Proceedings of the Study for an ep Facility for Europe*, U. Amaldi (ed.), p. 391. Hamburg, Germany (1979). Also in preprint DESY 79/48.
- [27] K.C. Höger, *Proc. Workshop on Physics at HERA*, W. Buchmüller and G. Ingelman (eds.), Vol. 1, p. 43. Hamburg, Germany (1992).
- [28] J.R. Forshaw and J.K. Storrow, *Phys. Lett. B* **268**, 116 (1991).
- [29] J.R. Forshaw and J.K. Storrow, *Phys. Rev. D* **46**, 4955 (1992).
- [30] D.K. Srivastava and K. Geiger, *Nucl. Phys. A* **647**, 136 (1999).
- [31] T. Sjöstrand et al., *PYTHIA 6.206 Manual*, 2002, available on <http://www.thep.lu.se/~torbjorn/Pythia.html>;
T. Sjöstrand et al., *Comput. Phys. Commun.* **135**, 238 (2001).
- [32] B. Andersson et al., *Phys. Rep.* **97**, 31 (1983).
- [33] CTEQ Coll., H.L. Lai et al., *Eur. Phys. J. C* **12**, 375 (2000).
- [34] M. Glück, E. Reya and A. Vogt, *Z. Phys. C* **53**, 127 (1992).
- [35] R. Brun et al., *Geant3*, CERN-DD/EE/84-1, 1987 (unpublished).
- [36] T. Namssoo, Ph.D. Thesis, University of Bristol, UK, 2006 (unpublished).
- [37] J.D. Morris, Ph.D. Thesis, University of Bristol, UK, 2007 (unpublished).

E_{jet} (GeV)	θ_c	ξ_{peak}	stat.	syst.
19	0.23	1.99	± 0.01	$+0.02$ -0.02
	0.28	2.10	± 0.01	$+0.01$ -0.01
	0.34	2.20	± 0.01	$+0.01$ -0.01
23	0.23	2.11	± 0.02	$+0.02$ -0.01
	0.28	2.21	± 0.02	$+0.02$ -0.01
	0.34	2.32	± 0.02	$+0.02$ -0.01
28	0.23	2.22	± 0.04	$+0.03$ -0.02
	0.28	2.34	± 0.03	$+0.02$ -0.02
	0.34	2.44	± 0.04	$+0.04$ -0.01
32	0.23	2.25	± 0.07	$+0.09$ -0.05
	0.28	2.36	± 0.06	$+0.10$ -0.03
	0.34	2.56	± 0.06	$+0.07$ -0.05
38	0.23	2.40	± 0.05	$+0.04$ -0.08
	0.28	2.50	± 0.08	$+0.07$ -0.18
	0.34	2.59	± 0.07	$+0.08$ -0.15

Table 1: ξ_{peak} values in the five E_{jet} bins using the three θ_c values. The statistical and systematic uncertainties are also given.

		ξ_{peak} analysis			ξ shape analysis		
E_{jet} (GeV)	θ_c	Λ_{eff} (MeV)	stat.	syst.	Λ_{eff} (MeV)	stat.	syst.
19	0.23	272	± 5	$^{+6}_{-8}$	304	± 4	$^{+7}_{-32}$
	0.28	280	± 4	$^{+5}_{-5}$	298	± 4	$^{+21}_{-25}$
	0.34	289	± 4	$^{+6}_{-5}$	303	± 3	$^{+15}_{-30}$
23	0.23	280	± 7	$^{+6}_{-7}$	307	± 6	$^{+10}_{-32}$
	0.28	291	± 9	$^{+3}_{-11}$	305	± 6	$^{+23}_{-32}$
	0.34	297	± 8	$^{+3}_{-9}$	301	± 5	$^{+26}_{-29}$
28	0.23	279	± 16	$^{+8}_{-11}$	285	± 12	$^{+8}_{-19}$
	0.28	282	± 14	$^{+8}_{-9}$	294	± 10	$^{+7}_{-29}$
	0.34	292	± 17	$^{+5}_{-17}$	287	± 9	$^{+29}_{-23}$
32	0.23	310	± 33	$^{+22}_{-41}$	298	± 15	$^{+25}_{-40}$
	0.28	321	± 29	$^{+14}_{-49}$	302	± 13	$^{+26}_{-41}$
	0.34	283	± 24	$^{+21}_{-28}$	286	± 14	$^{+28}_{-27}$
38	0.23	290	± 23	$^{+38}_{-16}$	311	± 15	$^{+13}_{-52}$
	0.28	301	± 37	$^{+48}_{-33}$	287	± 21	$^{+42}_{-32}$
	0.34	319	± 36	$^{+31}_{-38}$	297	± 17	$^{+21}_{-42}$

Table 2: Λ_{eff} extracted at the five E_{jet} points using the three θ_c values obtained from both the ξ_{peak} and ξ shape analyses. The statistical and systematic uncertainties are also given.

E_{jet} (GeV)	θ_c	κ^{ch}	stat.	syst.	theo.
19	0.23	0.54	± 0.01	+0.03 -0.02	+0.11 -0.09
	0.28	0.59	± 0.01	+0.03 -0.01	+0.12 -0.10
	0.34	0.63	± 0.01	+0.03 -0.02	+0.12 -0.10
23	0.23	0.56	± 0.01	+0.03 -0.02	+0.11 -0.09
	0.28	0.60	± 0.01	+0.04 -0.02	+0.12 -0.10
	0.34	0.63	± 0.01	+0.04 -0.02	+0.13 -0.10
28	0.23	0.55	± 0.01	+0.04 -0.01	+0.11 -0.09
	0.28	0.59	± 0.01	+0.04 -0.04	+0.11 -0.09
	0.34	0.61	± 0.01	+0.04 -0.02	+0.12 -0.10
32	0.23	0.56	± 0.02	+0.04 -0.04	+0.11 -0.09
	0.28	0.59	± 0.02	+0.04 -0.04	+0.11 -0.09
	0.34	0.61	± 0.02	+0.04 -0.03	+0.12 -0.10
38	0.23	0.56	± 0.03	+0.05 -0.06	+0.11 -0.09
	0.28	0.58	± 0.03	+0.04 -0.04	+0.11 -0.09
	0.34	0.61	± 0.03	+0.03 -0.05	+0.12 -0.10

Table 3: κ^{ch} values extracted at the five E_{jet} points using the three θ_c values. The statistical, systematic and theoretical uncertainties are also given.

ZEUS

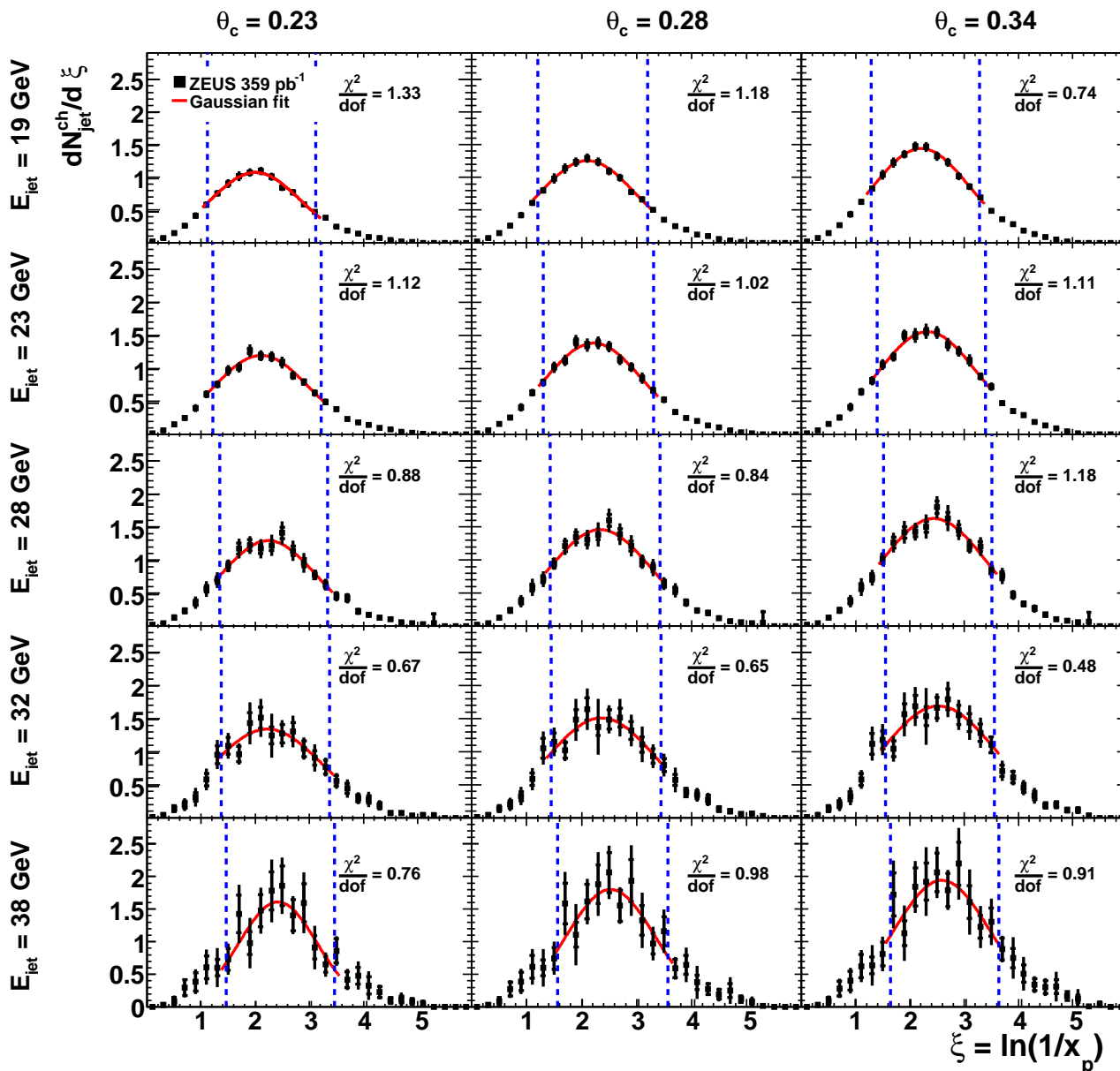


Figure 1: The ξ distributions in the five E_{jet} bins using the three θ_c values. The ZEUS data are shown by the solid squares. The inner error bars represent the statistical uncertainty. The outer error bars represent the statistical plus systematic uncertainties added in quadrature. Gaussian functions (solid line) have been fitted to the data within the regions indicated (dashed lines). The χ^2/dof of each fit is given on the plot.

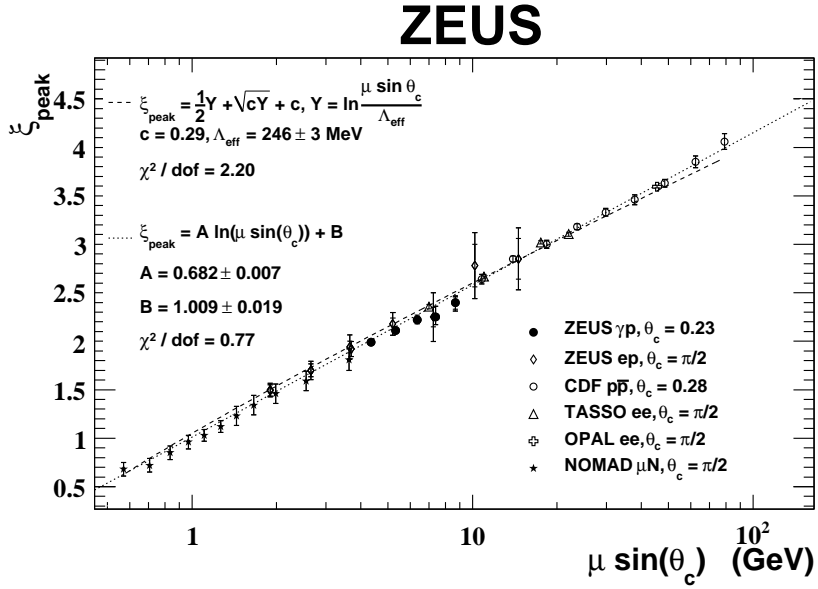


Figure 2: ξ_{peak} as a function of $\mu \sin(\theta_c)$, where μ denotes the characteristic energy scale for each specific process. The ZEUS γp data (solid circles) are shown along with ep data from the ZEUS collaboration (diamonds) and results reported by the OPAL (crosses), TASSO (triangles), NOMAD (stars) and CDF (open circles) collaborations. The inner error bars on the ZEUS points represent the statistical uncertainty. The outer error bars represent the statistical plus systematic uncertainties added in quadrature for all data sets. The data have been fitted with a straight line.

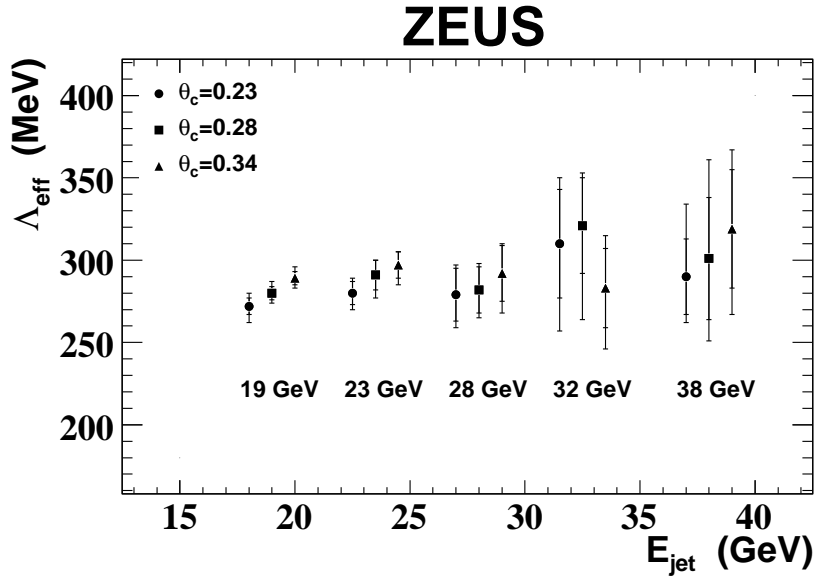


Figure 3: Λ_{eff} extracted at the five E_{jet} points using the three θ_c values. The ZEUS data are shown by the solid points. The inner error bars represent the statistical uncertainty. The outer error bars represent the statistical plus systematic uncertainties added in quadrature. The points have been shifted horizontally for clarity.

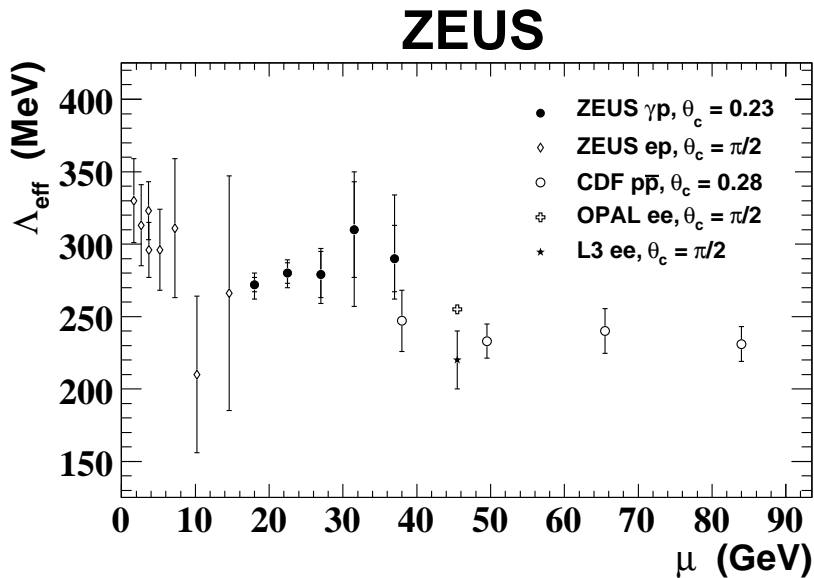


Figure 4: Λ_{eff} as a function of μ , where μ denotes the characteristic energy scale for each specific process. The ZEUS γp data are shown by the solid circles. Also shown are ep data from the ZEUS collaboration and results reported by the OPAL, L3 and CDF collaborations. The inner error bars on the ZEUS γp points represent the statistical uncertainty. The outer error bars represent the statistical plus systematic uncertainties added in quadrature for all data sets.

ZEUS

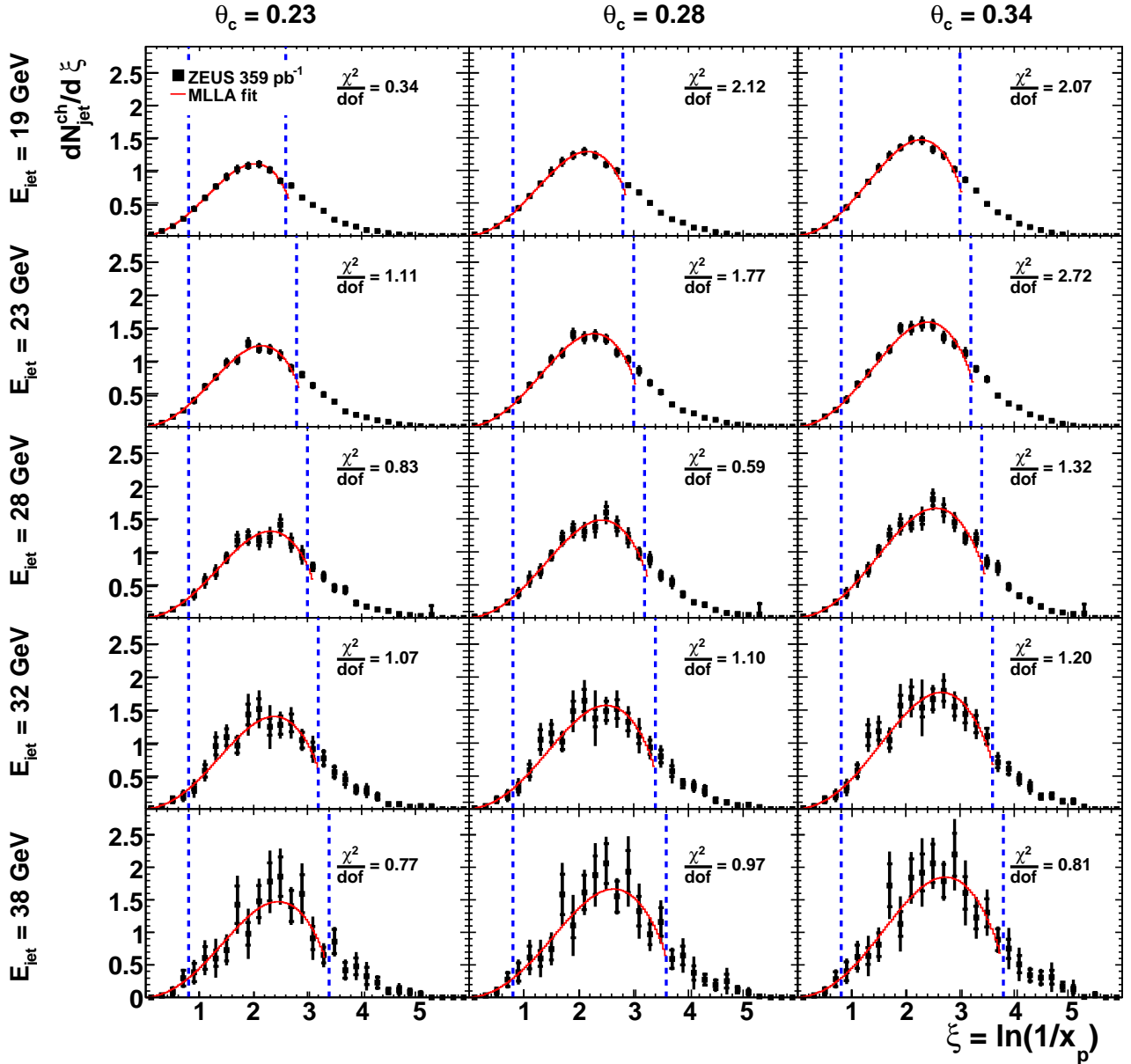


Figure 5: The ξ distributions in the five E_{jet} bins using the three θ_c values. The ZEUS data are shown by the solid squares. The inner error bars represent the statistical uncertainty. The outer error bars represent the statistical plus systematic uncertainties added in quadrature. The limited momentum spectrum predicted by the MLLA (solid line) has been fitted to the data within the regions indicated (dashed lines). The χ^2/dof of each fit is given on the plot.

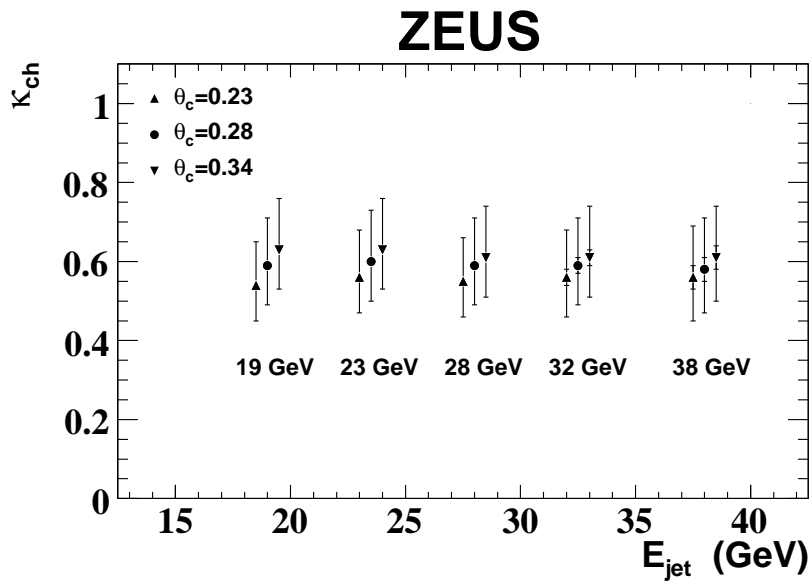


Figure 6: κ^{ch} extracted at the five E_{jet} points using the three θ_c values. The ZEUS data are shown by the solid points. The inner error bars represent the statistical uncertainty. The outer error bars represent the statistical, systematic and theoretical uncertainties added in quadrature. The points have been shifted horizontally for clarity.